# Fission decay of giant resonances in $^{238}$U excited in $\alpha$ scattering at small momentum transfer

B. Brinkmöller,* P. Decowski,† B. Marianski,‡ H. P. Morsch,§ D. Paul,** M. Rogge, R. Siebert,†† W. Spang,§ P. Turek, and L. Zemlo‡‡
*Institut für Kernphysik, Forschungszentrum Jülich GmbH, Postfach 1913, D-5170 Jülich, Germany*
(Received 23 October 1991)

Coincidences between inelastically scattered $\alpha$ particles and fission products from $^{238}$U have been measured with a 172 MeV $\alpha$ beam. Inelastically scattered $\alpha$ particles were measured at angles between 0° and 4°. The fission decay of the giant resonances, in particular, of the giant quadrupole resonance, is clearly observed in the coincidence data. Experimental fission probabilities are well described within the statistical model. The multipole strength, extracted from the angular distribution, is consistent with that obtained from singles $(\alpha,\alpha')$ measurements if a background due to multistep processes is taken into account.

PACS number(s): 25.85.−w, 25.55.Ci, 21.10.Re, 27.90.+b

## I. INTRODUCTION

Over the last decade a large amount of information on giant resonances has been collected and different resonance modes have been identified for heavy nuclei [1]. Also the decay properties of giant resonances were investigated. Of particular interest was the region of very heavy actinide nuclei for which fission decay of giant resonances can be studied. In the decay of the giant resonances into fission one can observe the transition between two different collective modes of motion, the fast small amplitude vibration of the giant resonances and the slow large amplitude fission mode. Several experiments have been performed to study fission decay of the isoscalar giant resonances exited in hadron and electron scattering [2–10].

In particular, different investigations have been made to study the fission decay of the isoscalar giant quadrupole resonance (GQR) in $\alpha$ scattering [2,5,6]. In heavy nuclei the decay of giant resonances should be predominantly statistical in nature, so it was quite puzzling that the fission decay of the giant resonance in $^{238}$U was not seen in an $(\alpha,\alpha' f)$ experiment [2]. It was concluded that the fission probability of the isoscalar GQR should be considerably smaller than that of the compound nucleus. In further studies quite contradictory results were found [5,6], but no definite conclusion could be reached. However, in recent ($^{17}$O,$^{17}$O′) coincidence studies on $^{238}$U clear indication was found [10] that the fission probability of the GQR is essentially identical to that for the underlying continuum.

There have been also studies of the fission decay of giant resonances in $(e,e'f)$ coincident experiments [7–9]. In electron scattering different giant resonances are excited with a dominant excitation of the isovector giant dipole resonance (GDR). Therefore, to distinguish decay from different giant resonance modes a careful study of the momentum dependence has to be performed. Recently such a study of the $^{238}$U$(e,e'f)$ reaction clearly indicated fission decay of the GQR [9]. A problem still remains, namely, that the monopole and quadrupole excitation cannot be distinguished, also isoscalar dipole and octupole strength. Further, from electron scattering one extracts information on the charge sum rule whereas from $\alpha$ scattering we obtain the isoscalar multipole strength. If there would be a strong mixing of isoscalar and isovector strength in heavy nuclei—this has been inferred from pion scattering [11]—then there could be large differences between $(\alpha,\alpha')$ and $(e,e')$ results. Therefore it is of large importance to get complementary results of good quality on giant resonance decay from electron and hadron scattering.

In order to solve the experimental discrepancies of giant resonance strength in the $^{238}$U$(\alpha,\alpha' f)$ reaction we investigated this reaction again, using a 172-MeV $\alpha$ beam at very small momentum transfers (corresponding to very small scattering angles $\Theta_{\alpha'}$ including 0°). At this beam energy giant resonances are strongly excited [12] which simplifies the detection of the giant resonance decay considerably. Furthermore, low multipolarities are selectively excited at small scattering angles. Thus, the combination of small angle measurement and high beam energy should yield unambiguous conclusions on the above problems.

*Present address: Institut für experimentelle Kernphysik, Universität Karlsruhe, D-7500 Karlsruhe, Germany.
†Present address: Physics Dept., Smith College, Northampton, MA 01063.
‡Present address: Institute for Nuclear Studies, Warsaw, Poland.
§Present address: Laboratoire National Saturne, F-91191 Gif-sur-Yvette Cedex, France.
**Present address: Dornier GmbH, D-7777 Friedrichshafen, Germany.
††Present address: Institute de Physique Nucleaire Orsay, F-91406 Orsay Cedex, France.
‡‡Present address: Institute of Nuclear Research, Warsaw, Poland.

 

## II. EXPERIMENTAL SETUP AND RESULTS

The experiment was performed using a $^{238}$U target with a thickness of 0.46 mg/cm$^2$ on a 0.05 mg/cm$^2$ carbon backing and a momentum analyzed $\alpha$ beam of 172 MeV from the Jülich cyclotron. To reduce background in the small angle measurements the beam was confined to a few mm×mrad using axial phase slits in the cyclotron center and special slits in the extraction path. The scattered $\alpha$ particles were momentum analyzed using the QQDDQ magnetic spectrometer BIG KARL [13]. The variable dispersion of the spectrometer was set to a rather small value of about (3.5 cm)$p$/(100$\Delta p$), where $p$ is the momentum of the measured particle. The spectrometer then covers an excitation energy range of about 40 MeV. The inelastically scattered $\alpha$ particles were detected in the focal plane by a 1-m long and 9-cm high drift chamber with position resolution in $X$ and $Y$ axis [14]. The total energy was measured in a 10-cm-thick plastic detector which gave clean particle separation. The efficiency along the focal plane was determined by measuring the elastic line at different positions. For the measurements of angles $\Theta_{\alpha'} \geq 2°$ the beam was stopped on the entrance slit of the spectrometer. In the $\Theta_{\alpha'}=0°$ run the beam was stopped on a carbon block between the two dipole magnets. At this position the $\alpha$ particles cannot be well focused, therefore the carbon block caused a large efficiency loss in the absolute yield, but also a cut in the low energy part of the spectrum (Fig. 1). The relative efficiency at 0° as a function of the focal plane position (upper part Fig. 1) was determined by measuring a spectrum at 3° under the same conditions (with carbon block) and comparing it to the spectrum taken without carbon block. The loss in the total inelastic yield at 0° was determined in the data analysis (see Sec. III) to be in the order of about 30%. The angles of the scattered particles were measured with an opening ±1.15° for $\Theta_{\alpha'}=0°$ and of ±1.15° horizontal and ±2.29° vertical for $\Theta_{\alpha'} \geq 2°$.

The fission products were measured in parallel plate avalanche detectors with active areas of 3×6 cm$^2$. The cathodes of the detectors were divided in 31 strips giving a position resolution of 2 mm in the reaction plane. Coincidences between identified $\alpha$ particles and fission products were recorded with a time resolution of about 5 ns which was sufficient to clearly separate prompt and random coincidences. For the $\Theta_{\alpha'}=0°$ run three detectors were placed in the reaction plane at positions shown in Fig. 2. Fission products were measured in the full reaction plane apart from angles close to the beam and parallel to the target surface. For the measurements with $\Theta_{\alpha'} \geq 2°$ only one detector was used covering an angular range from $\Theta_f = -40°$ to $-90°$. The target was oriented at an angle of 70° to the beam line to minimize shadowing of the fission detectors by the target frame.

The angular distribution of the fission fragments was obtained from the position spectra of the fission detectors. The resolution was limited to 3° due to the size of the beam spot on the target. From $(\alpha,\alpha' f)$ experiments at larger $\alpha'$ angles, it is known that the angular distribution of fission fragments, emitted from a nucleus at excitation energies just above the fission barrier, is peaked around the recoil axis [2,6]. However, at $\alpha'$ angles smaller than 4° the recoil direction changes rapidly with angle and the range of the recoil directions becomes more and more spread out within the angular acceptance of the spectrometer. In this case one observes an angular distribution which is no longer peaked, instead it is smeared out to such an extent that the spectra of the fission detectors show an almost isotropic behavior.

Efficiency corrected $\alpha'$ spectra coincident with fission decay are given in Fig. 3. In these spectra there is appre-

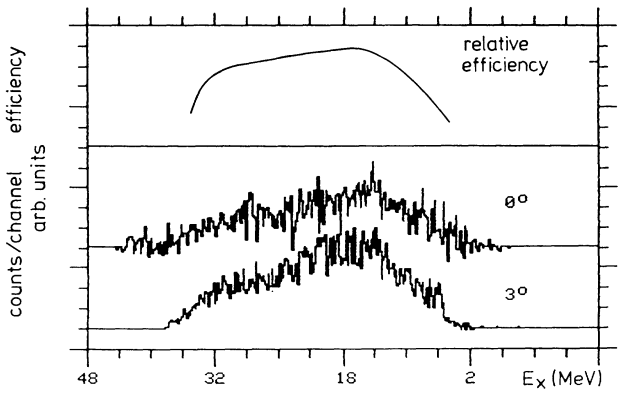


FIG. 1. Coincident $\alpha'$ spectra measured at 0° and 3° with a carbon block (lower part). From the comparison with the 3° spectrum, taken without carbon block, the efficiency for the 0° measurement has been determined (upper part).

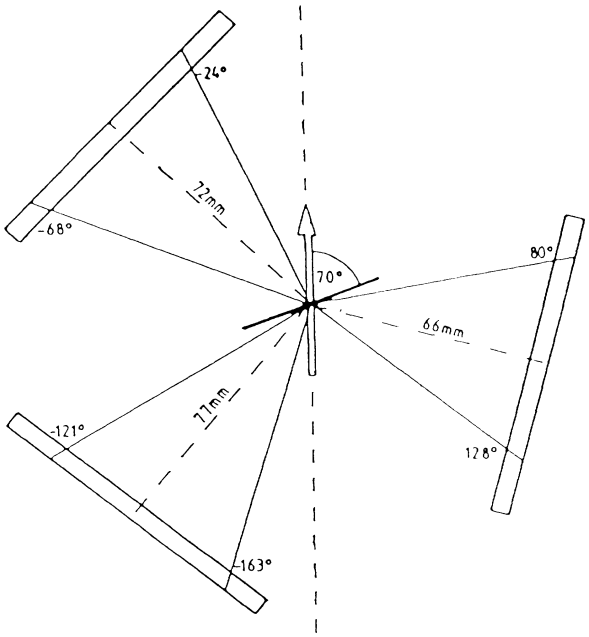


FIG. 2. Positions of the parallel plate avalanche detectors for measurement of the fission products. The beam direction is indicated by the arrow, also the target position is shown, which is oriented at an angle of 70° to the beam line.

ciable structure mainly due to threshold effects. The strong peak above 6-MeV excitation energy which is due to first chance fission and the structures above 13 and 19 MeV which are due to second and third chance fission decrease with angle. There are also indications of giant resonance effects. Most pronounced is a structure in the 3° and in the 4° spectrum in the energy region of 10 MeV where the GQR is located. An additional bump can be seen in the 0° spectrum in the energy region of 15 MeV. This may indicate the location of the giant monopole resonance.

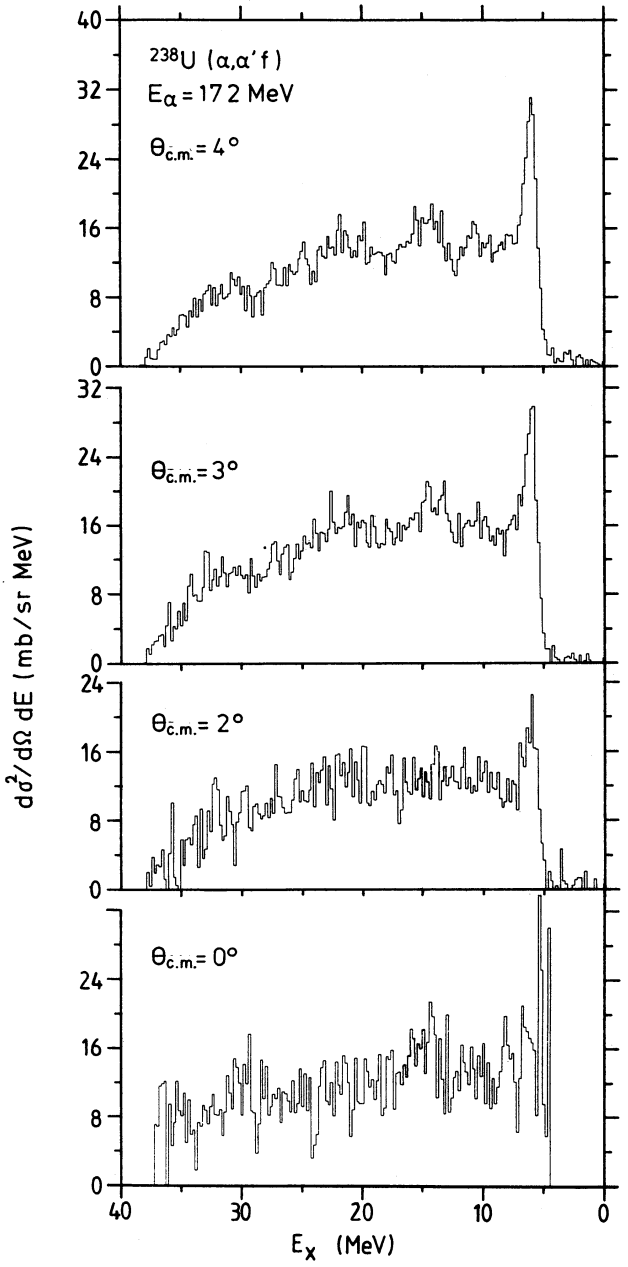


FIG. 3. Spectra of inelastic scattered $\alpha$ particles at angles of 0°, 2°, 3°, and 4° in coincidence with all fission products.

## III. MULTIPOLE DECOMPOSITION OF THE $(\alpha,\alpha')$ YIELD

Angular distributions of the $(\alpha,\alpha' f)$ yield in Fig. 3 are given in Fig. 4 for different bins of excitation energy. The data points show an angular behavior typical for a direct excitation mechanism with contributions of different multipoles. Therefore we made an attempt to decompose the inelastic yield by a number of multipole components. Such an analysis is quite common for electron scattering data, where the differential cross sections have a characteristic $L$ dependence [apart from $L=0$ and 2 and also $L=1$ and 3 ($T=0$) ambiguities]. In hadron scattering the situation is more complicated. Direct one-step excitation is generally not the dominant contribution in the spectra apart from the low energy discrete spectrum. At higher $E_x$ estimates of single scattering give only about $\frac{1}{3}$ of the total inelastic yield [15]. There are contributions, e.g., from particle knockout [16], which should set in at excitation energies above 12 MeV with increasing importance to large $E_x$. Another process which is expected to contribute significantly to the continuum yield in $\alpha$ scattering is multiple (or multiphonon) excitation, since the $\alpha$-nucleon interaction at our beam energy is very strong [17]. The yield due to these more-step processes should give a rather flat angular distribution which may be approximated by the behavior of direct one-step calcu-

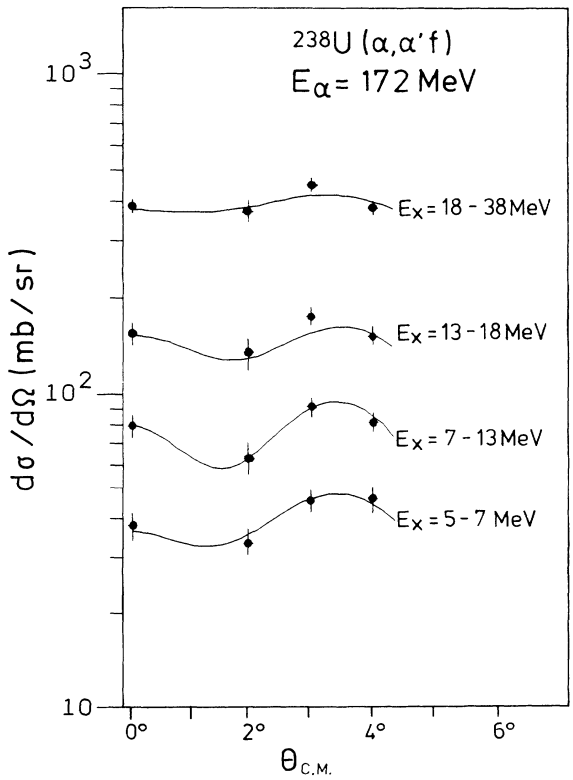


FIG. 4. Angular distributions of the differential cross sections of the $\alpha'$ yield for different bins of excitation energies. The lines indicate the result of a multipole decomposition using DWBA calculations (see text).

lations using larger $L$ values. However, this implies that the sum rule strengths for larger $L$ values must be overexhausted by a large amount (in total in the order of 3) in such a multipole description of the $(\alpha,\alpha')$ cross section.

As direct excitation of low $L$ values is relatively large at small momentum transfers it appears conceivable to perform such a multipole decomposition of the inelastic yield based on reliable direct one-step calculations which describe well the properties of direct inelastic $\alpha$ scattering. For this we used distorted wave Born approximation (DWBA) calculations in which folding form factors are used (Fig. 5). For details of the calculations see Refs. [18,19]. These calculations show that at higher $E_x$ already the $L=2$ component has a rather flat angular distribution which may as well describe the behavior of the other processes discussed above.

For the $L=1$ excitation one has different contributions in $\alpha$ scattering: There should be isoscalar dipole excitation at $1\hbar\omega$ and $3\hbar\omega$ energies as well as isovector GDR excitation [20]. The latter is due to Coulomb excitation but also nuclear effects are present giving rise to interference effects. The resulting angular distribution in the angle region of interest is not very different from that obtained for isoscalar dipole excitation. Therefore, for convenience, the angular shape of isoscalar excitation was used.

The DWBA calculations show a sharp diffraction pattern for low angular momenta (Fig. 5). For the lowest excitation region the different multipole contributions up to $L=4$ are very different which should yield an unambiguous multipole decomposition. For higher excitation energies the $L$ characteristics become less clear and lead to larger ambiguities for $L \geq 3$.

A general solution of the problem shows very large ambiguities. In order to reduce this, the contributions of the low multipoles were taken to be consistent with the sum rule strengths found in Refs. [18,19] assuming that at

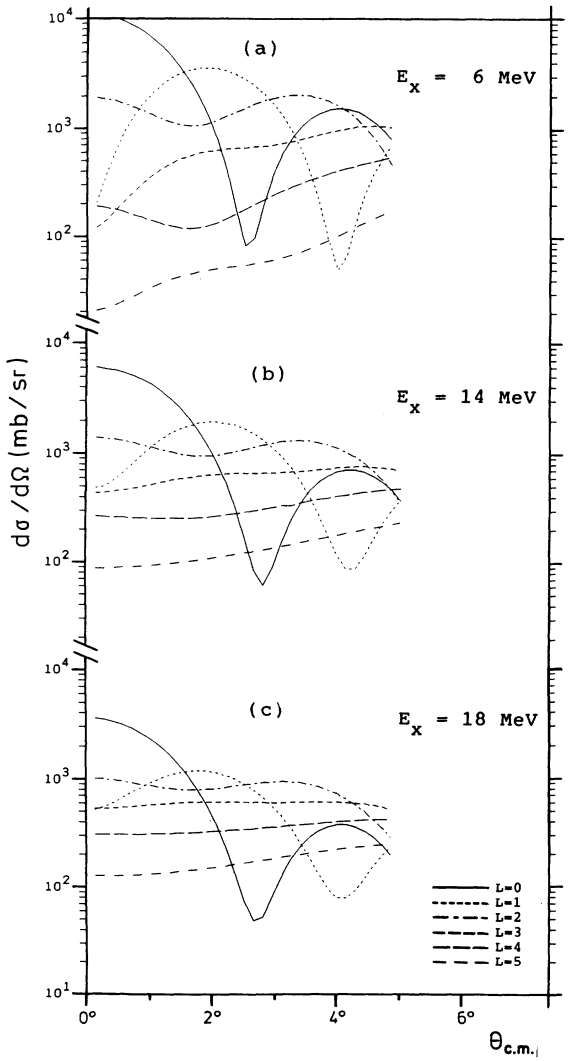


FIG. 5. Differential cross sections of multipolarity $L=0-5$ for inelastic $\alpha$ scattering from $^{238}$U at three different excitation energies calculated within a DWBA approach.

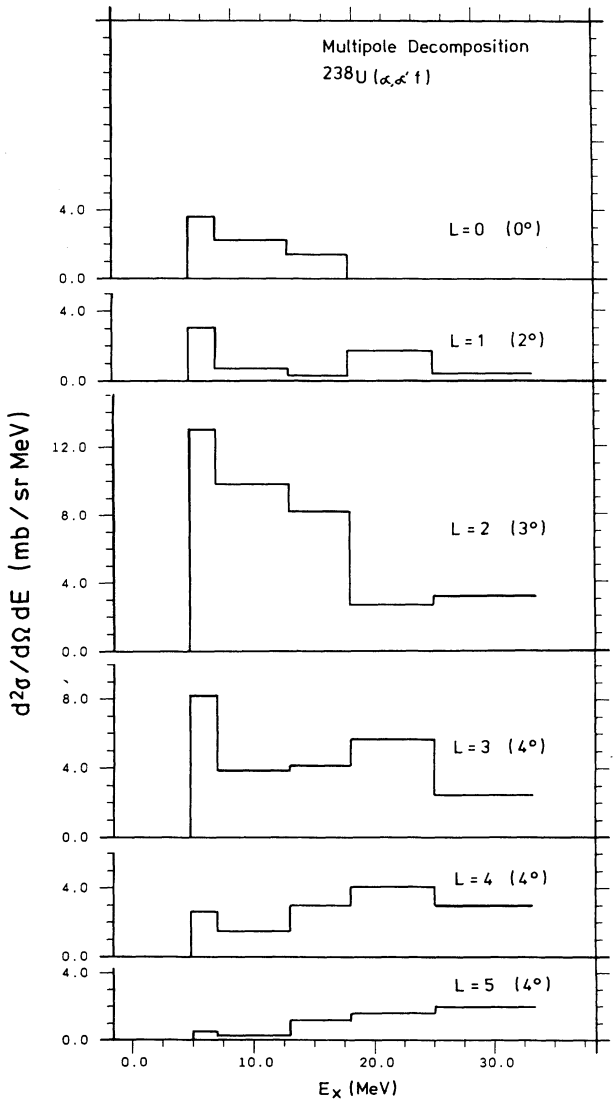


FIG. 6. Multipole strengths for different $L$ values extracted from the $(\alpha,\alpha' f)$ yield.

least the sum rule strengths for the giant resonances are observed. Also, it was required that the higher $L$ contributions, which approximate the background calculations, do not change rapidly from one energy bin to the other (continuity approximation for the background yield).

Due to the special problems with the 0° measurement (see Sec. II) we could not extract reliable absolute cross sections for this angle. To achieve this the following procedure was used: From the DWBA calculations in Fig. 5 it is obvious that the main contribution of monopole strength to the total yield is at 0°. This monopole strength is concentrated in the GMR excitation which in $^{238}$U is split into two components located at 9.3 (30%) and 13.7 MeV (65%) [18]. Therefore, the monopole contribution in the energy bin of 13–18 MeV can be well estimated using the sum rule strength exhausted by the GMR component at 13.7 MeV. The contribution of the higher multipoles to the cross section at 0° is given by the fits to the data points at 2°, 3°, and 4°. Comparing the estimated with the measured cross section in this energy bin we obtained a factor of 1.3 which was used to normalize the absolute cross section of the whole 0° spectrum. The systematical error which is caused by the above procedure is not contained in the error bars of the data points in Fig. 4 which give only the statistical error.

The result of the multipole decomposition is shown in Fig. 6. It gives a good description of the angular distributions which is indicated by the lines in Fig. 4. The $L=2$ contribution clearly dominates the yield. However, as discussed above, the $L=2$ angular distribution is already rather flat, therefore this contribution covers a large amount of the background yield at larger $E_x$.

## IV. FISSION PROBABILITIES AND STATISTICAL MODEL ANALYSIS

Experimental fission probabilities $p_f^{\exp}$ have been derived from the spectra taken at 3° and 4° by dividing the $^{238}$U$(\alpha,\alpha' f)$ coincidence yields by the $^{238}$U$(\alpha,\alpha')$ cross section [18]. Whereas the measured spectra for $(\alpha,\alpha' f)$ have very little instrumental background, the $(\alpha,\alpha')$ yield contains a significant background due to light contaminants in the target and slit scattering. Correctly normalized background spectra have been subtracted from the $(\alpha,\alpha')$ yield as well as multiple scattering contributions estimated according to Ref. [15] to obtain the $^{238}$U$(\alpha,\alpha')$ spectra. For a scattering angle of 4° $p_f^{\exp}$ is shown in Fig. 7. This result was normalized to reproduce the experimentally known fission probability of $p_f^{\exp}\approx 0.18$ found in previous $(\alpha,\alpha' f)$ experiments at excitation energies of 10–12 MeV [2,6]. It shows very pronounced thresholds due to first, second, and third chance fission.

We compared the experimental fission probability $p_f^{\exp}$ with calculations using the statistical model code PACE2, a modified version of JULIAN-PACE [21]. In this approach the fission probability $p_{fL}$ is calculated independently for each $L$ and $p_f$ is obtained by using the following relations:

$$p_{fL}=\frac{\sigma_L(\alpha,\alpha' f)}{\sigma_L(\alpha,\alpha')}\,,$$
$$p_f=\frac{\sum_L[\sigma_L(\alpha,\alpha')p_{fL}]}{\sum_L \sigma_L(\alpha,\alpha')}\,. \tag{1}$$

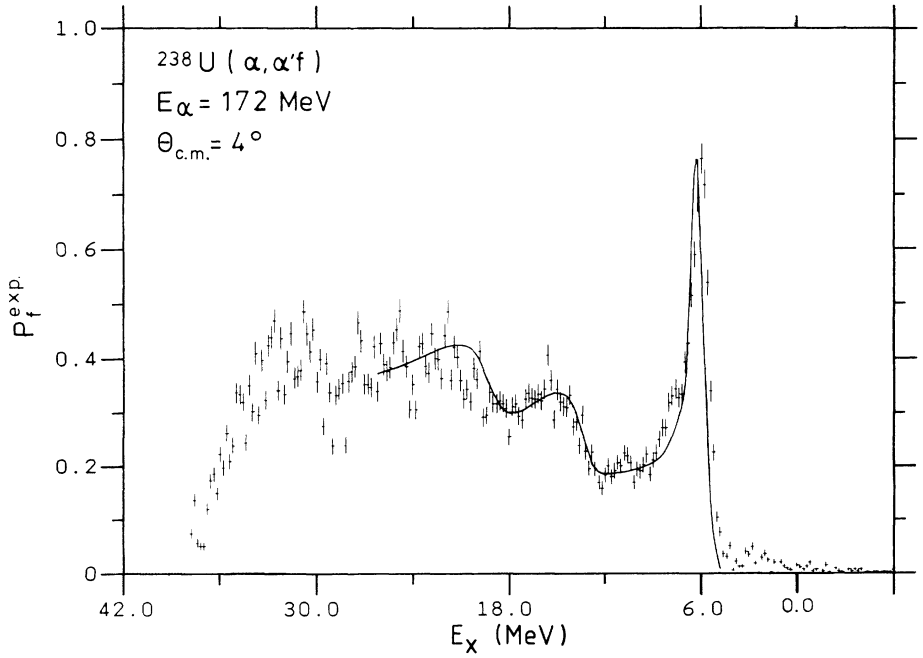


FIG. 7. Experimental fission probability at a scattering angle of 4°. The solid line indicates the result of a statistical model calculation with the code PACE2 discussed in Sec. IV.

For the decay of uranium isotopes at 6–30-MeV excitation energy only neutron emission and fission are important. To calculate neutron emission, transmission coefficients taken from optical model calculations and a semiempirical level density formula for excitation energies above the pairing gap [22] are used in PACE2. However, as PACE2 was written to calculate the decay of compound nuclei at high excitation energies, a refined description of the fission process had to be introduced to adopt it for calculations in the excitation energy region of interest here.

The fission barrier is commonly defined by an inverted oscillator potential. The parameters defining the barrier are the height $E_{\text{barr}}$ and the width $\hbar\omega$. With these parameters the transmission coefficient $T_f(J^\pi,E_x)$ for a state with given $J^\pi$ at excitation energy $E_x$ can be obtained by integrating over all states of the transition nucleus at barrier deformation with the same spin and parity [23]:

$$T_f(J^\pi,E_x)=\int \frac{\rho_{\text{barr}}(\varepsilon,J^\pi)}{1+\exp[-2\pi(E_x-E_{\text{barr}}-\varepsilon)/\hbar\omega]}d\varepsilon \quad (2)$$

where $\rho_{\text{barr}}$ is the density of states at barrier deformation.

In many detailed studies it was found that the fission barrier for actinide nuclei consists of two barriers $A$ and $B$ where the inner barrier $A$ is slightly higher than the outer barrier $B$. The transition coefficient for this double humped barrier can be calculated using the transition coefficients $T_A$ and $T_B$ of the two barriers [24]:

$$T_f=\frac{T_A T_B}{T_A+T_B} . \quad (3)$$

However, the effect of the barrier structure only affects fission directly at threshold. For excitation energies above the barrier the influence of the lower barrier becomes less important. Also, the necessary input parameters are not known well enough to allow such a calculation. Therefore we chose to calculate the $p_{fL}$ for a single barrier using Eq. (2).

In the calculation the same level density $\rho_{\text{barr}}$ was used for the ground state and the transition nucleus, i.e., $a_f/a_n=1$, where $a_n$ and $a_f$ are the level density parameters for the ground state and transition nucleus, respectively. The best description of the experimental results was obtained with barrier widths of $\hbar\omega=0.6$ MeV. To describe the fission probability $p_f$ for the whole range of excitation energy measured in this experiment, fission of $^{238}$U, $^{237}$U, and $^{236}$U is important and to a lesser degree also of $^{235}$U and $^{234}$U. The fission barriers $E_{\text{barr}}$ were fitted to reproduce the experimental fission probability $p_f^{\text{exp}}$ in Fig. 7.

Although it is not possible to compare our results for the heights of the single fission barriers directly with the parameters of double humped fission barriers [24], the latter put some constraints on the range of barrier heights that can be considered reasonable. The values for $E_{\text{barr}}$ obtained by our fit are generally higher than the values for $E_{\text{barr}}(A)$, the higher of the two barriers of the double humped fission barrier. The difference is largest for the even-even nuclei. This is consistent with the assumption of larger pairing gaps on top of the barrier. As the intrinsic level density increases at barrier deformation [24] one can assume that the following relation holds:

$$E_{\text{barr}}(A)<E_{\text{barr}}<E_{\text{barr}}(A)+P(Z)_{\text{barr}}+P(N)_{\text{barr}}-P(Z)-P(N) , \quad (4)$$

where $P(N)$ and $P(Z)$ are the neutron and proton pairing gaps for the nucleus with ground state deformation and $P(N)_{\text{barr}}$ and $P(Z)_{\text{barr}}$ are the pairing gaps for the transition nucleus.

In Table I the barrier heights $E_{\text{barr}}$ extracted from this experiment are given together with the parameters

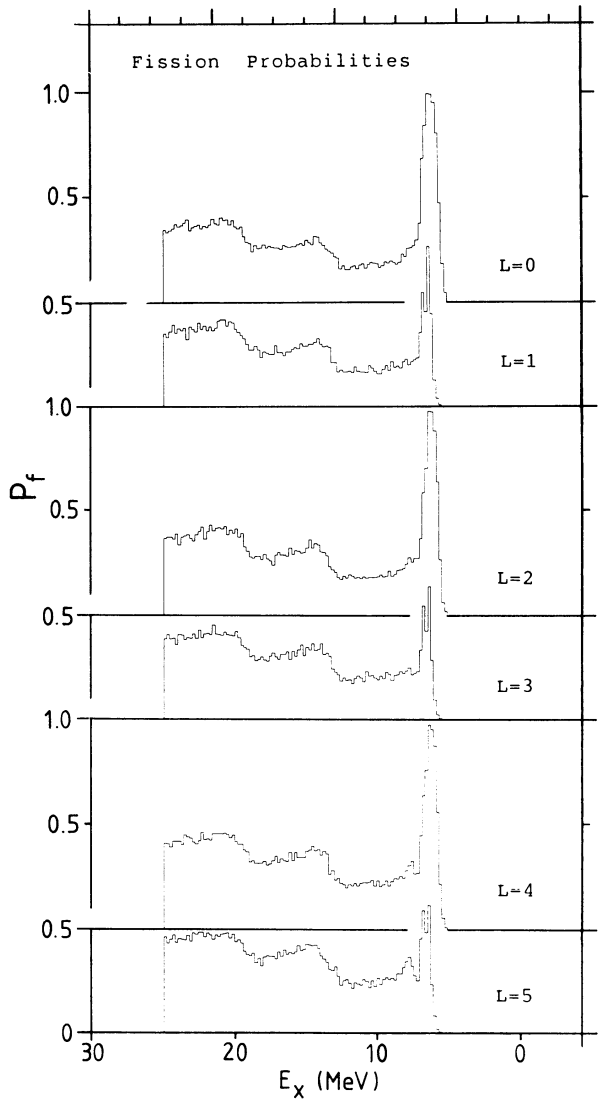


FIG. 8. Calculated fission probabilities $P_{fL}$ for various values of $L$. Significant differences are found only in the barrier region.

TABLE I. Barrier heights extracted from this experiment together with the parameters describing the double humped fission barrier (see text) taken from Ref. [27]. All values are given in MeV.

| Nucleus | $E_{\text{barr}}$ | $\hbar\omega$ | $E_{\text{barr}}(A)$ | $E_{\text{barr}}(B)$ | $\hbar\omega(A)$ | $\hbar\omega(B)$ |
|---|---|---|---|---|---|---|
| $^{238}$U | 6.3 | 0.6 | 5.7 | 5.7 | 1.0 | 0.6 |
| $^{237}$U | 6.1 | 0.6 | 6.28 | 6.08 | 0.8 | 0.52 |
| $^{236}$U | 6.4 | 0.6 | 5.63 | 5.53 | 1.04 | 0.6 |
| $^{235}$U | 6.2 | 0.6 | 6.15 | 5.9 | 0.8 | 0.52 |
| $^{234}$U | 6.5 | 0.6 | 5.6 | 5.5 | 1.04 | 0.6 |

describing the double humped fission barrier taken from Ref. [24]. The relationship given in Eq. (4) holds for the description of the fission decay of all nuclei entering the analysis of our data.

Another input for the statistical model calculation is the angular momentum distribution of the start ensemble. For this, the results of the multipole decomposition of Sec. III were used. The calculations showed that the fission probabilities in the region of the giant resonances above $E_x = 9$ MeV are nearly independent from the choice of the start ensemble (see Fig. 8).

In contrast to this, the fission probabilities in the region of the barrier depend very much on the multipolarity. This is already seen in the spectra taken at different scattering angles in Fig. 3. It is also apparent if one compares the experimental fission probability $p_f^{\text{exp}}$ in Fig. 7, which goes up to $\approx 0.8$, with measurements at larger scattering angles where the fission probability at the barrier is about a factor of two smaller [6]. Furthermore, the barrier yields depend strongly on the barrier width and details of the level structure above the barrier.

It is obvious that our model, which was chosen to describe the fission probability a few MeV above the barrier, cannot describe the details of the barrier shape. Our value for $E_{\text{barr}}$ is 0.5 MeV higher than that for $E_{\text{barr}}(A)$ for $^{238}$U. As a consequence the calculated fission peak is shifted to higher excitation energies compared with the experimental peak.

However, the introduction of discrete states of the transitional nucleus below the pairing gap into the calculation improves the description for excitation energies above the barrier considerably (see Fig. 9). If one assumes only the ground state rotational band, fission of odd $L$ states is forbidden close to the fission threshold. Using this assumption and the results of the multipole decomposition a peak value of $p_f = 0.45$ and a sharp gap in the coincidence yield at 7-MeV excitation energy is predicted for $\theta_{\alpha'} = 4°$ (short dashes in Fig. 9).

Levels of a different type are needed to fill up this gap. From the multipole decomposition of the $(\alpha,\alpha' f)$ yield a strong $L = 3$ and also $L = 1$ component is indicating fission from negative parity bands. Including an odd parity mass vibrational band a few hundred keV above the barrier [25] in the calculations improves the description

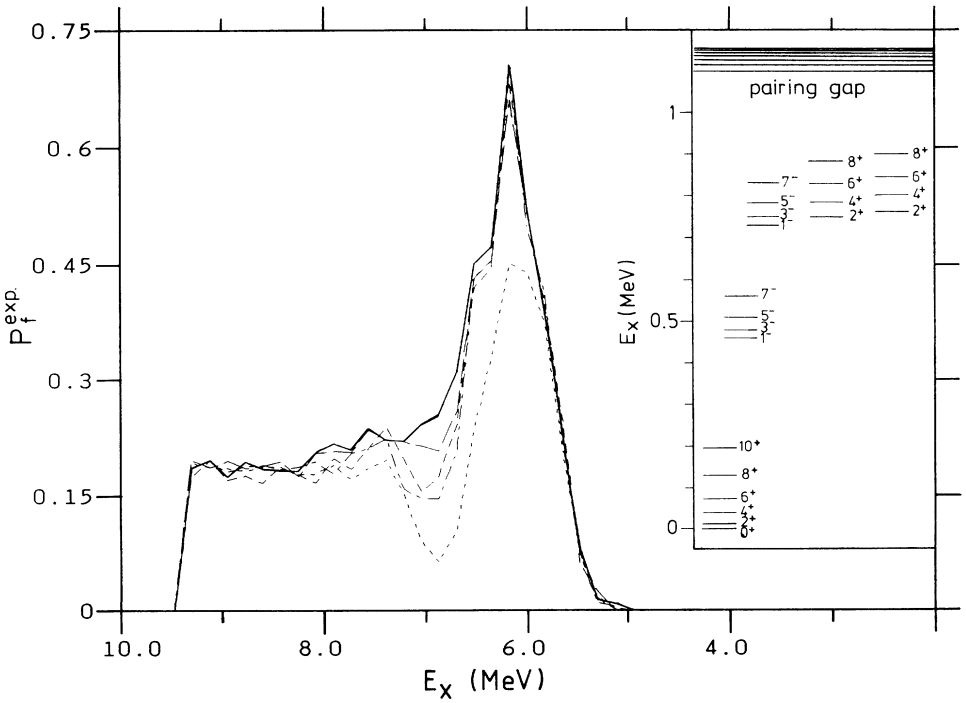


FIG. 9. Fission probability $P_f$ in the barrier region calculated from the statistical model taking into account different bands above the fission saddle point (inset). Taking into account only the lowest $0^+$ band yields $P_f$ given by the short dashed line. Including a negative band at $\sim$450 keV above the barrier gives the dot-dashed line whereas the inclusion of a second odd parity band yields the dashed line. Taking into account all bands indicated in the inset sums up to the solid line.

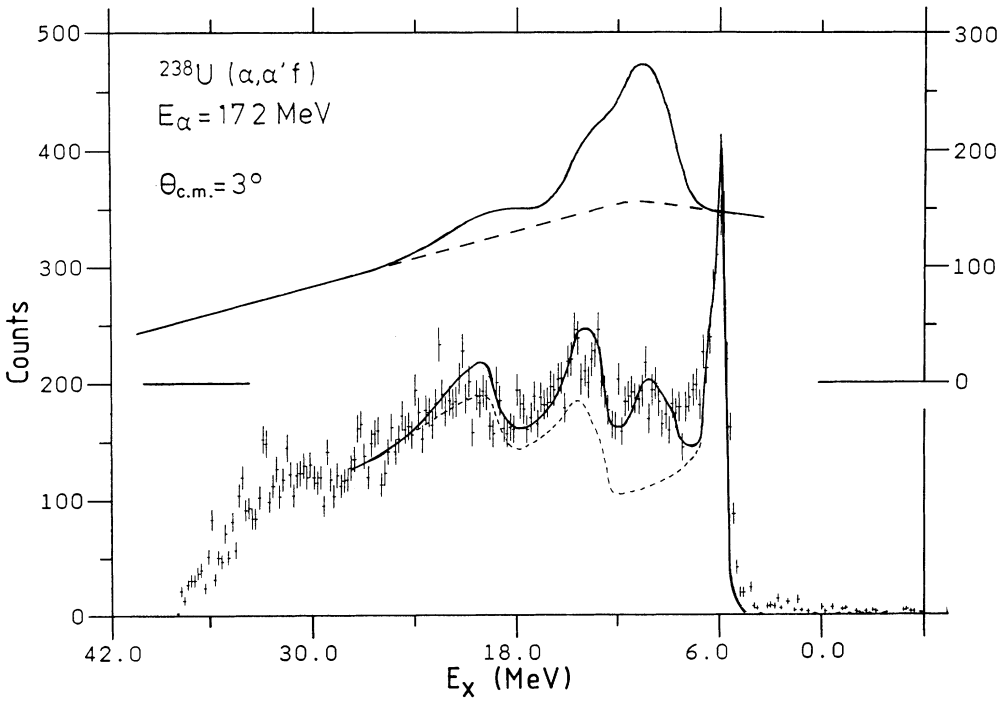


FIG. 10. Coincident 3° $\alpha'$ spectrum (lower part) in comparison with the singles $(\alpha,\alpha')$ spectrum (upper part) which shows very pronounced giant resonance structure. The solid line in the lower part is obtained by multiplying the singles spectrum (solid line, upper part) with the fission probability $P_f$, whereas the dashed line in the lower part is obtained by multiplying the background yield (dashed line, upper part) with $P_f$.

of the barrier and the gap considerably (dot-dashed line in Fig. 9). The inclusion of the three other vibrational bands, as indicated in Fig. 9, gives a smooth fall off the fission peak consistent with the experimental observation.

The final result for $p_f$ is given by the solid line in Fig. 7 and in Fig. 9. Between about 7 and 8 MeV the data show a structure which cannot be reproduced by this simplified calculation. In the region above 8 MeV the description does not depend on the models used to fit the barrier. Thus, the good overall description of the experimental fission probability $p_f^{\text{exp}}$ clearly supports the assumption of dominant statistical decay in heavy nuclei, also from the giant resonances.

The total effect of the giant resonances in the fission coincidence spectra can be shown in another way directly in the fission spectra. Figure 10 shows the coincident $(\alpha,\alpha'f)$ spectrum and on top the singles $(\alpha,\alpha')$ spectrum at a scattering angle of 3°. Using the theoretical fission probability $p_f$ the fission spectrum can be calculated directly. The solid line in the lower spectrum is obtained by multiplying the full inelastic response with $p_f$ whereas the dashed line gives only the contribution due to the background component.

The difference between solid and dashed line shows the effect of the giant resonances on the fission spectrum. As already seen from the experimental spectra in Sec. II the peak around 10 MeV is entirely due to the decay of the giant quadrupole resonance. The effect of the GMR and GDR is also quite apparent around 14 MeV.

## V. MULTIPOLE STRENGTH DISTRIBUTION OF THE INELASTIC YIELD

From the multipole decomposition of the $(\alpha,\alpha'f)$ yield (Sec. III) and the fission probabilities discussed in Sec. IV, the final multipole strength distributions can be derived. The results of such an analysis are shown in Fig. 11 together with the indications of the location of giant resonances and their respective widths from $(\alpha,\alpha')$ experiments [18]. The extracted distributions show pronounced structure for low multipolarities consistent with the location of giant resonances and the extracted sum rule strengths (see Table II) are in agreement with previous results [18,19]. However, for $L \geq 2$ the total strengths are much larger than the energy weighted sum rule (EWSR) limits. This indicates strong contributions of processes other than one-step direct excitation. As this is already the case at low excitation energies below particle emission threshold this extra yield can be understood only as contribution from multiple inelastic excitation. In the following the contributions of the different $L$ components are discussed.

$L=0$. The location and strength of the $L=0$ yield is in good agreement with the GMR results from $(\alpha,\alpha')$ measurements [18,19] which gave indication of a splitting of the GMR in actinides. The strength is consistent with the full energy weighted sum rule. In Ref. [26] different results on the GMR have been published based on small angle scattering results showing only a broadening of the GMR in $^{238}$U. However, in the analysis in Ref. [26] a

subtraction technique is applied assuming that in the difference spectrum (0° minus 3° spectra) only the $L=0$ component is seen. This is very questionable. By taking into account the GQR contribution from our folding calculations in Sec. III, which is not negligible, the spectra in Ref. [26] are well described consistent with a splitting of the GMR in Ref. [18].

$L=1$. Isovector dipole excitation is quite weak in $\alpha$ scattering. The extracted cross section is in remarkable agreement with the estimated yield covering the full EWSR strength. At higher excitation energies there is additional $L=1$ strength. This is consistent with excitation of the isoscalar giant dipole compression mode, the squeezing mode of the nucleus [19] covering a sum rule strength of about 70%. At the fission threshold indication for low energy dipole (LED) strength is found which may be interpreted as isoscalar dipole excitation located at an energy of $1\hbar$. This is consistent with the isoscalar $L=1$ strength found in $^{208}$Pb [27].

TABLE II. Fractions of the EWSR exhausted by the total multipole strengths which were obtained by the multipole decomposition of Sec. III.

| | Fraction of EWSR (in %) | | | | | |
|---|---|---|---|---|---|---|
| $E_x$ (MeV) | $L=0$ | $L=1$ | $L=2$ | $L=3$ | $L=4$ | $L=5$ |
| 5–7 | 2 | 2 | 5 | 7 | 2 | 2 |
| 7–13 | 58 | 30 | 111 | 40 | 23 | 13 |
| 13–18 | 22 | 11 | 133 | 52 | 41 | 27 |
| 18–38 | | 20 | 288 | 179 | 198 | 171 |
| Total | 82 | 63 | 537 | 278 | 264 | 213 |

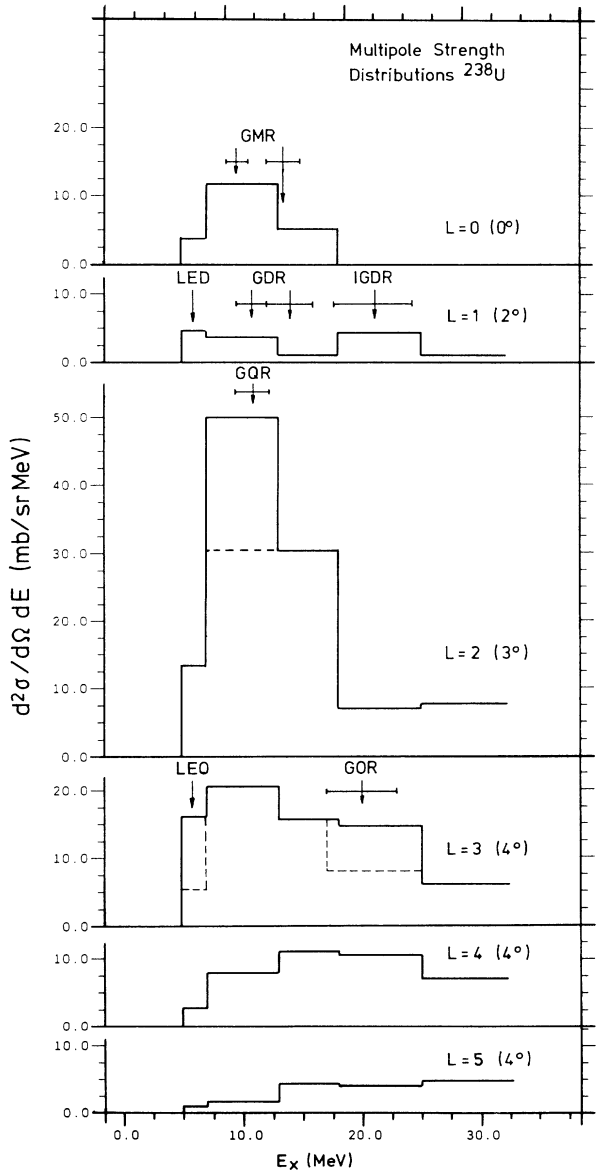


FIG. 11. Multipole strengths distributions for different $L$ values. The arrows indicate expected low energy structures and known giant resonances from Ref. [18] with their widths indicated. The two arrows for GMR and GDR indicate the splitting of the resonances into two components.

$L=2$. Concerning the GQR our data present clear evidence for fission decay of this resonance. The strength distribution has a strong peak at the GQR energy but also a wide $L=2$ contribution towards larger $E_x$. The area above the dashed line in Fig. 11 corresponds to the sum rule strength ($\approx$70%) observed in Refs. [18,19]. The broad $L=2$ strength has a sum rule strength exceeding by far the EWSR and thus must be due to the background processes discussed above.

$L=3$. The strength extracted has a rather broad distribution, with a sum rule strength exceeding the energy weighted sum rule limit by a large amount. In Fig. 11 the location of the GOR is shown with the strength from Ref. [18] indicated by the area above dashed line. Also, the strong excitation of $L=3$ states at the fission threshold (Fig. 6) is consistent with the excitation of the low energy octupole (LEO) resonance known for many nuclei. Due to the strong energy dependence of the fission probability $p_f$ above threshold (Fig. 8) and the background contributions at high $E_x$, more definite conclusions on the octupole yield are not possible.

$L=4$. The distributions of $L=4$ and 5 are quite flat and show total yields in excess of the energy weighted sum rules. Because of large ambiguities in the multipole decomposition a statement on the direct multipole strength cannot be made.

Our results for the multipole decomposition can be compared with $(e,e'f)$ experiments. In the measurement of Refs. [7,8] too small a $L=2$ strength is extracted in the GQR region. Only in the new $(e,e'f)$ study [9] in which the $L$ distribution and also the form factors were fitted simultaneously is $L=2$ strength found which is consistent with the EWSR strength from $(\alpha,\alpha')$ [18,19]. Also, the strength found in the region of $\sim$14 MeV is in good agreement with the monopole strength found in our experiment. However, only from our $(\alpha,\alpha'f)$ experiment is it possible to separate the monopole and quadrupole components.

The comparison with older $\alpha$ scattering coincidence experiments indicates that the experiment of Ref. [2] was

performed at too low an energy to see the effect of giant resonances. From beam energies of 120–170 MeV giant resonance cross sections increase by more than a factor of 2, further the yield increases towards smaller angles. Nevertheless, because of the large fission threshold effects, the giant resonance effects in the fission coincidences can only be revealed by a comparison with statistical model calculations.

Considering the results from the ($^{17}$O,$^{17}$O′) studies in Ref. [10] there is a remarkable agreement with our results concerning the fission decay of the GQR. However, in Ref. [10] only weak evidence for the fission decay of the GMR is found. This can be understood by the fact that monopole excitation is less pronounced in heavy ion collisions, except maybe at $\Theta_{lab}=0°$ which was not measured.

Concerning the multipole strength in the region of the barrier, the extracted 5% $L=2$ strength is about a factor of 2 larger than that extracted from $(e,e'f)$ [7–9]. This may indicate that already in the barrier region there are contributions from multiple excitation which is reasonable to assume. A strong $L=3$ excitation at the barrier is in agreement with $(e,e'f)$ results [8,9].

For the background, qualitative features are revealed which give more insight into its structure: it starts right at the fission threshold, clearly below the three-body $p$ and $n$ thresholds. This supports the picture that it is mainly due to multiple excitation (consistent with the conclusions in Ref. [17]) rather than due to breakup processes which start at the particle thresholds. So it is conceivable to draw a background line which starts at rather low energy. For the higher multipoles the strength covers between two and four sum rules which is in good agreement with the estimates given in Ref. [15].

## VI. CONCLUSIONS

In our experiment, fission decay of giant resonances has been studied which were excited in small angle $\alpha$ scattering. Fission decay of the giant quadrupole resonance is clearly observed and described quantitatively assuming statistical decay. This solves the long standing problem of fission decay of this state.

A first attempt has been made to perform a multipole decomposition of the whole coincident $(\alpha,\alpha'f)$ cross section without subtracting background. From the multipole expansion, results on giant resonance structures and the features of the background are obtained. The location and strength of giant resonances extracted in our analysis are consistent with the singles $(\alpha,\alpha')$ measurements and recent results of $(e,e'f)$ studies.


[1] H. P. Morsch, in *Proceedings of the Niels Bohr centennial conference on Nuclear Structure 1985*, edited by R. Broglia, G. B. Hagemann, and B. Herskind (Elsevier, New York, 1985), p. 433 and references therein.

[2] J. v. d. Plicht, M. N. Harakeh, A. van der Woude, P. David, and J. Debrus, Phys. Rev. Lett. **42**, 1121 (1979); J. v. d. Plicht, M. N. Harakeh, A. van der Woude, P. David, J. Debrus, H. Janszen, and J. Schulze, Nucl. Phys. **A346**, 349 (1980).

[3] J. D. T. Arruda Neto and B. L. Berman, Nucl. Phys. **A349**, 483 (1980), and references therein.

[4] H. Ströher, R. D. Fischer, J. Drexler, K. Huber, U. Kneissl, R. Ratzek, H. Ries, W. Wilk, and H. J. Maier, Phys. Rev. Lett. **47**, 318 (1981); Nucl. Phys. **A378**, 237 (1982).

[5] F. E. Bertrand, J. R. Beene, C. E. Bemis, F. E. Gross, D. J. Horen, J. R. Wu, and W. P. Jones, Phys. Lett. **99B**, 213 (1981).

[6] H. P. Morsch, M. Rogge, P. Decowski, H. Machner, C. Sükosd, P. David, J. Debrus, J. Hartfield, H. Janszen, and J. Schulze, Phys. Lett. **119B**, 315 (1982).

[7] D. H. Dowell, L. S. Cardman, P. Axel, G. Bolme, and S. E. Williamson, Phys. Rev. Lett. **49**, 113 (1982).

[8] K. A. Griffeon, P. J. Countryman, K. T. Knöpfle, K. van Bibber, M. R. Yearian, J. G. Woodworth, D. Rowley, and J. R. Calarco, Phys. Rev. Lett. **53**, 2382 (1984).

[9] T. Weber, R. D. Heil, U. Kneissl, W. Pecho, W. Wilke, H. J. Emrich, T. Kihm, and K. T. Knöpfle, Phys. Rev. Lett. **59**, 2028 (1987).

[10] R. L. Auble, J. R. Beene, F. E. Bertrand, J. L. Blaneknship, D. J. Horen, J. Lissantti, and R. L. Varner, Phys. Rev. C **41**, 2620 (1990).

[11] S. J. Seestrom-Morris, C. L. Morris, J. M. Moss, T. A. Carey, D. Drake, J. C. Douse, L. C. Land, and G. S. Adams, Phys. Rev. C **33**, 1847 (1986).

[12] H. P. Morsch, M. Rogge, P. Turek, C. Sükösd, and C. Mayer-Böricke, Phys. Rev. C **20**, 1600 (1979).

[13] S. A. Martin, A. Hardt, J. Meissburger, G. P. A. Berg, U. Hacker, W. Huerlimann, J. G. 'M. Römer, T. Sagefka, A. Retz, O. W. B. Schult, K. L. Brown, and K. Halbach, Nucl. Instrum. Methods **A214**, 281 (1983).

[14] L. G. Atencio, G. P. A. Berg, P. v. Brentano, B. Brinkmöller, G. Hlawatsch, J. Meissburger, C. F. Moore, C. L. Morris, D. Paul, J. G. M. Römer, M. Rogge, P. v. Rossen, T. Sagefka, S. J. Seestrom-Morris, and L. Zemlo, Nucl. Instrum. Methods A **242**, 95 (1985).

[15] H. P. Morsch, J. Phys. C **4**, 185 (1984).

[16] P. Decowski, H. P. Morsch, M. Rogge, P. Turek, L. Zemlo, G. Gaul, R. Glasow, B. Ludewigt, R. Santo, and W. Schumacher, Phys. Lett. **141B**, 49 (1984).

[17] H. P. Morsch, D. Cha, and J. Wambach, Phys. Rev. C **31**, 1715 (1985).

[18] H. P. Morsch, M. Rogge, P. Turek, C. Mayer-Böricke, and P. Decowski, Phys. Rev. C **25**, 2939 (1982).

[19] H. P. Morsch, P. Decowski, M. Rogge, P. Turek, L. Zemlo, S. A. Martin, G. P. A. Berg W. Hürlimann, J. Meissburger, and J. G. M. Römer, Phys. Rev. C **28**, 1947 (1983), and references therein.

[20] P. Decowski and H. P. Morsch, Nucl. Phys. **A377**, 261 (1982), and references therein.

[21] A. Gavron, Phys. Rev. C **21**, 230 (1980).

[22] A. Gilbert and A. G. W. Cameron, Can. J. Phys. **43**, 1446 (1965).

[23] D. L. Hill and J. A. Wheeler, Phys. Rev. **89**, 1102 (1953).

[24] S. Bjornholm and J. E. Lynn, Rev. Mod. Phys. **52**, 725 (1980).
[25] P. A. Dickey and P. Axel, Phys. Rev. Lett. **35**, 501 (1975).
[26] S. Brandenburg, R. de Leo, A. G. Drentje, M. N. Harakeh, H. Janszen, and A. van der Woude, Phys. Rev. Lett. **49**, 1687 (1982).
[27] P. Decowski, H. P. Morsch, and W. Benenson, Phys. Lett. **101B**, 147 (1981).